Hydrothermal-electrochemical deposition of semiconductor thin films: the case of CuIn(Al)Se2 compound

UNIVERSITÀ DEGLI STUDI DI TORINO

Hydrothermal-Electrochemical Deposition of Semiconductor Thin Films: The case of CuIn(Al)Se_2 Compound

by

Yadolah Ganjkhanlou , Valentina Crocellà, Mahmood Kazemzad, Gloria Berlier, Touradj Ebadzadeh, Iman Safaee, Alireza Kolahi, Amir Maghsoudipour

J Mater Sci: Mater Electron (2017) 28:15596–15604

DOI 10.1007/s10854-017-7446-9

Hydrothermal-Electrochemical Deposition of Semiconductor Thin Films: The case of $CuIn(Al)Se_2$ Compound

Yadolah Ganjkhanlou [1,2*], Valentina Crocellà[2], Mahmood Kazemzad[1], Gloria Berlier[2], Touradj Ebadzadeh[1], Iman Safaee[1], Alireza Kolahi[1], Amir Maghsoudipour[1]

1-Materials and Energy Research Center, P.O. Box 14155-4777, Tehran, Iran
2- Department of Chemistry, NIS and INSTM Reference Centre, Università di Torino, Via P. Giuria 7, 10125 Torino, Italy
Corresponding author's email: Yadolah.ganjkhanlou@unito.it

Abstract
Electrochemical deposition of $CuIn(Al)Se_2$ thin film from quaternary aqueous solution of Cu, In, Al and Se salts has been carried out at different temperatures (25, 55 and 80 ^oC) and it was found that optical properties, crystallinity and phase purity of the as-deposited $CuIn(Al)Se_2$ films are enhanced at higher temperature. Consequently, electrodeposition of $CuIn(Al)Se_2$ under hydrothermal condition at high temperature (120 ^oC) and at different potentials is performed. The characterization of the obtained layers indicates that single phase chalcopyrite film could be deposited by synergism of the electrodeposition and hydrothermal methods at optimized deposition potential (-600 mV). Superior photoconductivity has also been observed in case of electrodeposited layer at 120 ^oC (hydrothermal condition). More interestingly, post annealing of CIAS thin film prepared by developed procedure at 200 ^oC (ambient atmosphere) results in dense microcrystalline layer with a photoconductivity 300 times higher than the sample deposited at room temperature.

Keyword: Hydrothermal, Electrochemical deposition, $CuIn(Al)Se_2$ alloy, Thin film, Solar cell.

1. Introduction
Thin film solar cells are known as the second generation of solar cells which have high potential for competing with silicon-based solar cells [1,2]. Among them, solar cells with chalcopyrite absorber layer have the highest reported solar energy conversion efficiency (more than 22%) [3]. Industrially, solar cells with chalcopyrite copper indium diselenide absorber layer have been fabricated by one or multi-step vacuum thermal evaporation techniques [4]. High processing cost and environmental problems of these methods limit the production scale of this type of solar cells. Indeed, high vacuum processing condition, inefficient materials utilization and the requirement of post selenization (application of highly toxic Se compounds in gas phase) cause these restrictions. Research is now focused on finding new clean and economical deposition techniques to overcome these limitations [5]. One of the promising methods introduced for this purpose is electrodeposition of copper indium diselenide (CIS) layers and other related materials such as copper indium gallium diselenide (CIGS) and copper indium aluminum diselenide (CIAS). Main limitations of this technique are undesired stoichiometry of obtained layers as well as the necessity of post heat treatment in inert (high cost) or selenium (toxic environment) atmosphere [6].

CIS and its related materials are among the most studied materials for fabrication of thin film solar due to its direct band gap and high light absorption coefficient. The band gap of quaternary semiconductors from this family (e.g. CIGS, $CuIn(S, Se)_2$ and $Cu(In, Al)Se_2$ (CIAS) could be tuned by their composition [7]. The partial substitution of selenium with S is one method for band gap enhancement however phase segregation

is favored in the presence of S [8]. On the other hand, a fraction of indium could be substituted with Ga or Al to increase the band gap of CIS (1.04 eV). In comparison with gallium, lower amounts of aluminum incorporation could tune the band gap of CIS phase toward the desired value of 1.4 eV due to higher band gap of $CuAlSe_2$ (2.7 eV) in comparison with $CuGaSe_2$ (1.8 eV) [9,10] and considering the Vegard's law [11]. Lower material cost and less distortion in the CIAS crystals in comparison with CIGS (due to low Al content) are the main advantages of CIAS as absorber materials for thin film solar cell applications in comparison with CIGS compound [10,12,13]. Consequently, CIAS is also studied as potential absorber layer of thin film solar cell. High-efficiency CIAS solar cell with efficiency more than 16.9% has been reported by Marsillac et al. [10]. Electrodeposition of CIAS has recently been reported by different research group however still more researches in this area are needed for preparation of CIAS thin films with desired stoichiometry [14-19].

Mechanism and effective parameters of semiconductors electrodeposition should be studied for enhancement of the CIAS deposition [6,20]. Electrodeposition could be easily utilized for fabrication of binary semiconductor like CdTe, nevertheless electrodeposition of ternary and quaternary semiconductors is relatively difficult. Padrós et al. [21] applied three potential pulsed electrodeposition method for fabrication of $CuInSe_2$ thin film and they obtain almost single phase chalcopyrite at low concentration. In addition to deposition parameters, complexing agents could also be implemented to shift the reduction potential of noble species toward the reduction potential of active species and obtaining better chemical composition. Citric acid is one of the well known complexing agent utilized during electrodeposition of CIS and CIGS in order to adjust the diffusion flux of copper and selenium [22-24]. Additionally, citric acid, can also buffer the aqueous electrolytes and reduce pH fluctuation on the cathode, which suppress the possible metal oxide and hydroxides formation. As reported in the literature, the presence of citric acid as well as supporting electrolyte could improve the homogeneity and the smoothness of deposited layer [22]. In approach known as *induced co-deposition*, reduced noble species utilized to induce the reduction of active species in potential less negative than reduction potential of active ions. This phenomenon is also known as Kroger's mechanism. Formation energy of compound provides enough energy to induce the reduction of active species in positive potential [25]. In order to increase the induced electrodeposition, the concentration of active species should be higher than noble species in electrodeposition electrolyte. However, electrodeposition of binary semiconductors is less sensitive to the unavoidable fluctuation of electrolyte composition and potential in case that this mechanism takes action. Induced electrodeposition is the main mechanism occurring during the electrodeposition of active metal chalcogenides (for example In_2Se_3, Ga_2S_3, CdTe) [20,26] while it is not considerable in the case of noble metal chalcogenide (for instance CuSe) due to the lower less difference of noble metal reduction potentials (Cu^{2+}) and chalcogen containing ions (HSO_3^-, $HSeO_3^-$ and $HTeO_2^+$) [25]. CIAS contains both noble (Cu) and active (In, Al) metals and therefore all of mentioned approaches (controlling the electrodeposition parameters and induced electrodeposition) should be utilized to obtain desired stoichiometry during electrodeposition.

Main advantages and limitations of the electrodeposition technique for quaternary semiconductors are described by Saji et al. [6] in their recent review paper. Two main limitations of this method are low crystallinity of the as-deposited layer as well as undesired stoichiometry of the obtained film. Synergism of the electrodeposition with other solution-based techniques is suggested by them as a good strategy for enhancing the resultant film properties. In the current work, the synergism of the hydrothermal and the electrodeposition techniques has been utilized as an efficient method for the preparation of CIAS thin film with enhanced properties. The improvement of the film microstructure, as a result of the applied technique, was monitored by field emission scanning electron microscopy (FE-SEM), X-ray diffraction (XRD), Photoconductivity and Raman spectroscopy techniques.

2. Experimental

2.1. Preparation method

Cleaned foils of stainless steel (SS) [27,28] and CdS coated fluorine-doped tin oxide (FTO) (sheet resistance of initial FTO layer was 8-10 Ω/sq) with an active area of 0.5 cm^2 have been implemented as substrate for electrodeposition of CIAS. Prior to deposition, SS foils have been polished with alumina past (grain size <0.1 μm) and then washed with acetone and deionized water for several times. The FTO substrate was also washed with surfactant, acetone and deionized water and then heat treated at 250 ^oC prior to utilization. The CdS layer was prepared on the FTO substrate in optimized condition as reported in ref. [29]. The CdS coated FTO was selected as substrate for preparation of main samples as it is suitable for fabrication of superstrate solar cell [30]. The electrodeposition electrolyte consists of sulfate salts of Cu (5 mM), In (20 mM), Al (20 mM), and 10 mM of SeO_2 beside 100 mM of NaCl and 200 mM of citric acid, all dissolved in MilliQ water. The pH of the solution has been adjusted by application of NaOH and H_2SO_4 solutions. Three different layers were prepared on SS substrates at different temperatures (25, 55 and 80 ^oC) for a preliminary investigation of the temperature effects. Then, additional layers were prepared on CdS coated FTO substrate at room temperature as well as 120 ^oC under hydrothermal condition with different electrodeposition potentials. Table 1 lists the names and conditions for preparation of all electrodeposited layers.

Table 1 Conditions of the electrodeposition of the prepared samples

Sample Name	Deposition Potential	Substrates type	Temperature (^oC)
CIAS-SS-RT	-700 mV	Stainless Steel	RT
CIAS-SS-55	-700 mV	Stainless Steel	55
CIAS-SS-80	-700 mV	Stainless Steel	80
RT-700	-700 mV	CdS coated FTO	RT
HT-600	-600 mV	CdS coated FTO	120-hydrothermal
HT-700	-700 mV	CdS coated FTO	120-hydrothermal

The electrodeposition was performed in a 20 ml beaker with an electrochemical workstation (IviumStat Instruments) using three electrode systems. A substrate, graphite electrode and an Ag/AgCl (saturated with KCl) electrode were applied as the working electrode, counter and reference electrodes, respectively. Before the electrodeposition, cyclic voltammetry (CV) measurement has been performed several times to study the deposition mechanism of CIAS with scan rates of 50 mV/S. Then, the co-deposition has been carried out in chronoamperometry configuration in fixed potential (determined by CV analyses) on clean substrate for 10 min (to have thickness of about 2-3 μm based on ref. [15]). A special autoclave (S. Fig.1), with three electrodes inside the reactor, has been employed to perform the electrodeposition in hydrothermal condition. A graphite bar with a cross-section of 0.5 mm^2 was used as quasi-reference electrode instead of Ag/AgCl reference electrode, as it is not possible to employ reference electrode at high temperature under hydrothermal condition. The CV curves recorded in autoclave were calibrated by comparing it with the CV curves recorded for same electrolyte in standard condition. CV curves recorded at room temperature and 120 ^oC show that co-deposition potential lowered (from -650 mV to -500 mV) at elevated temperatures (e.g. S. Fig. 2). In the current work, deposition potential has been optimized to obtain best possible stoichiometry (slightly negative than co-deposition potential, S. Fig. 2). The prepared samples were characterized by field emission scanning electron microscopy (FE-SEM), Energy-dispersive X-ray spectroscopy (EDS) and X-ray

diffractometry analysis. The X-ray diffraction (XRD) patterns were recorded by Philips DW3710 instrument using Cu Kα radiation operating at 50 KV and 250 mA in the 2θ range of 15-120º. FE-SEM and EDS investigations were carried out using a ZEISS electron microscope (EVO50) occupied with EDS (Oxford INCA Energy 200). Raman spectra were recorded by using a Renishaw Raman Microscope spectrometer. An Ar^+ laser emitting at 514 nm was used as exciting source, in which the output power was limited to 0.5% (100% power = 2 mW at the sample) in order to avoid sample damage (our results showed that higher power of laser changes the film crystallinity and composition specially in ambient atmosphere). The photons scattered by the sample were dispersed by a grating monochromator of 1800 (or 1200) lines/mm and simultaneously collected on a CCD camera; the collection optic was set at 50x objective. The spectra were obtained by collecting 40 acquisitions (each of 20 s).

The photoconductivity assessments were simply performed in a 30 ml beaker containing 1 M solution of NaCl under chopping illumination of white LED (2 W). NaCl solution has been selected as electrolyte for photo-response investigation due to the high mobility of containing ions. The prepared thin film (active area of 0.5 cm^2) was applied as working electrode in three electrode system and graphite electrode as well as Ag/AgCl (saturated with KCl) electrode were utilized as the counter and reference electrodes, respectively. Cyclic voltammetry from -1.0 V to 1.0 V (or -0.5 to 0.5 V) was recorded under chopped illumination to determine the conductivity type (P or N) of the layer (e.g. S. Fig 3). Then, the constant potential of -1.0 V was applied to investigate the current changes under chopped illumination (photo-response of sample).

3. Results and discussion

As mentioned in the previous section, the electrochemical deposition of CIAS from quaternary solution in presence of NaCl and Citric acid at initial pHs of 4 and at different temperatures (25, 55 and 80 ºC) has been performed. The X-ray diffraction analyses of the layers (Fig. 1A) demonstrate that their crystallinity has been greatly enhanced by increasing the temperature of the deposition (in fact, it is possible to observe that the intensity of the diffraction lines increases and, at the same time, their broadening decreases). Moreover, it can be observed that at room temperature other low crystalline binary phases of a Cu-Se system are present in the deposited layers and, with increasing the temperature up to 55 ºC, the crystallinity of all phases is enhanced. At T= 80 ºC, the amounts of others phases are decreased and intensity of the diffraction lines of chalcopyrite phase are increased (Fig. 1A). The as-deposited layer is also characterized by means of Raman spectroscopy for a better discrimination of the different phases (especially the low crystalline ones). The Raman spectra of the as-deposited layer at different temperatures are depicted in Fig. 1B. Two main bands could be observed in the Raman spectra. The band at 183 cm^{-1} is related to the A1 vibrational mode of the CIAS chalcopyrite phase which can also be assigned to the ordered defect compound in the CIS system (special phase formed by formation of ordered defects in CIS chalcopyrite phase [31]) due to the overlapping of their vibration modes. It should be considered that with aluminum incorporation, the A1 band of pure CIS chalcopyrite phase (175 cm^{-1}) shifts to higher frequency [32,33]. Ordered defect compound is known as Cu-Au phase in literature due to similarity of structure to Cu-Au system [32]. Another band, observed at 241 cm^{-1}, is related to in-plane resonance of Se phase [32]. Raman spectra clearly indicate that, by increasing the temperature, the intensity of the band related to the chalcopyrite phase increases and, at the same time, its broadening decreases, due to the higher crystallinity. Similar results have been reported on other semiconducting materials [34-36].

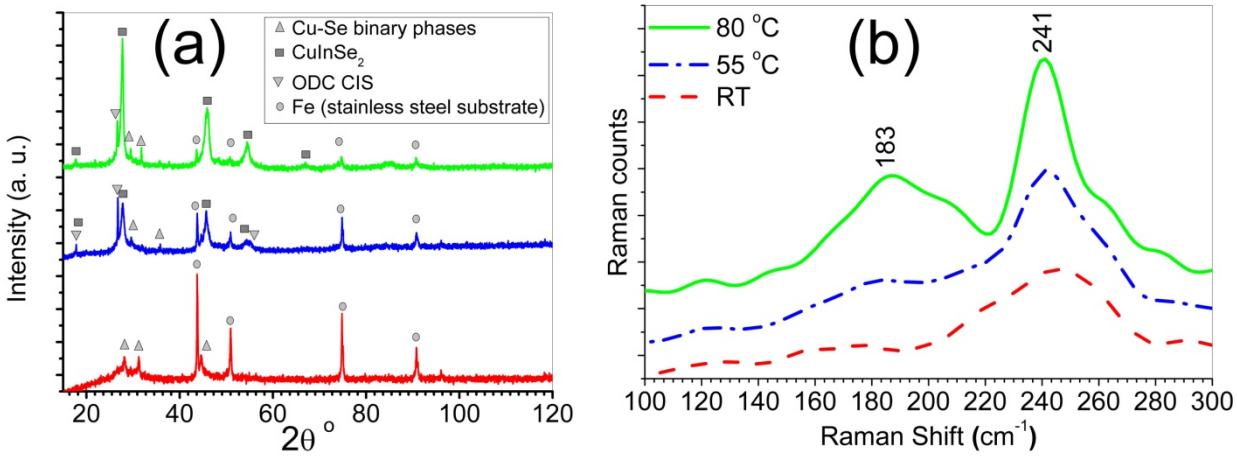

Fig. 1 Effect of temperature on the phase content and crystal structure of the electrodeposited CIAS film from the quaternary base solution: a) X-ray diffraction patterns b) Raman spectra.

The morphological investigation of the layers (see SEM images in Fig. 2) illustrates that at higher temperature a laminar growth is dominant, while a mix of spherical and laminar morphologies is obtained at lower temperature. A laminar morphology is also occasionally observed in the literature [37,38]. Considering the EDS results, it can be observed that with increasing the temperature, the stoichiometry improves toward the desired composition (Fig. 3). It was reported that the Cu-deficient stoichiometry of CIS phase is the best composition for having the P-type conductivity and the desired band gap [4]. EDS results also indicate that higher incorporation of In and Al as active metal can be obtained at elevated temperature. The band gap of the deposited layer calculated from diffuse reflectance UV-Vis-NIR spectra by Tauc method using Kubelka-Munk function as absorbance coefficient [39-41] is illustrated in Fig. 4. It is evident that with increasing the temperature from room temperature to 80 °C the band gap increases from 1.05 eV to 1.17 eV. The incorporation of Al as active metal is the main reason for this band gap enhancement.

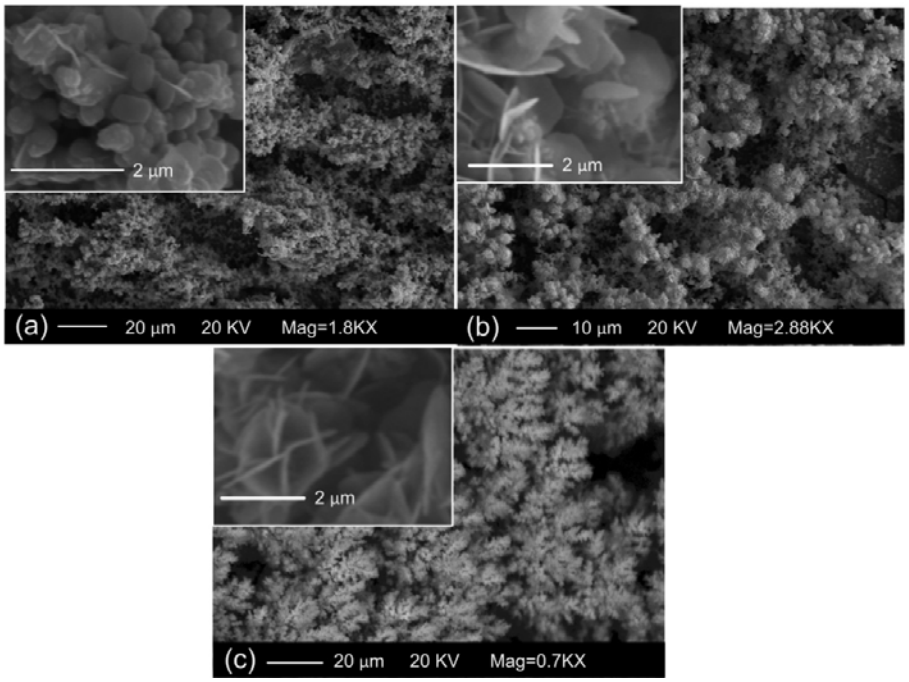

Fig. 2 FE-SEM images of as electrodeposited CIAS thin films from quaternary solution of Cu (5 mM), In (20 mM), Al (20 mM) and Se (10 mM) containing the citric acid (200 mM) and NaCl (100 mM) as complexing agent and supporting electrolyte respectively, at temperature of a) 25 °C b) 55 °C c) 80 °C.

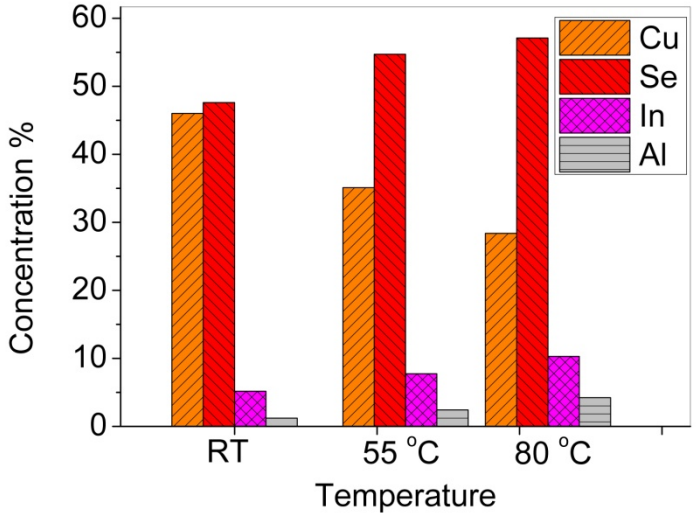

Fig. 3 Effect of temperature on stoichiometry of electrodeposited CIAS layers from quaternary solution

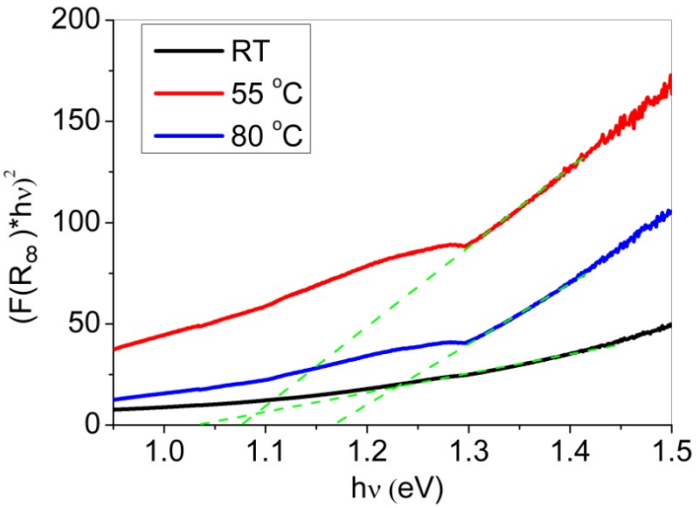

Fig. 4 Temperature effect on the band gap of electrodeposited CIAS thin films

All the above-reported results, obtained by XRD and Raman techniques as well as UV-Vis-NIR and EDS, clearly point out that the crystallinity, the bandgap, the chemical composition and phase purity of the deposited film are enhanced by increasing the temperature. However, to achieve temperatures higher than that of the water boiling point, it is necessary to work in hydrothermal conditions and consequently, a sealed electrochemical cell with permanence of at least 5 MPa was designed to carry out electrodeposition at temperature higher than 100 ºC.

Employing the above-mentioned cell, layers of CIAS were electrodeposited on a CdS coated FTO substrate in hydrothermal condition at 120 ºC. After the optimization of the electrodeposition potential, a dense, single phase chalcopyrite layer with enhanced crystallinity can be obtained, as shown by the SEM and XRD data depicted in Figs. 5 and 6. Electrodeposition was performed by applying two different constant potential -700 mV and -600 mV. At potential of -700 mV, the stoichiometry of the deposited layer lacks from the active metals (In and Al), while at -600 mV the composition is close to the desired stoichiometry of CIAS layer (Table 2) [42,43]. At the deposition potential of -700 mV an interesting morphology is observed (Fig. 5b), consisting of aggregates of planar CIAS (the planar growth is clear in the magnification) with some

fractality. This type of morphology, with a lot of porosity, is not desired for solar cell thin films, but may have potential application in photocatalysis for instance in water splitting applications by solar irradiation, in which, in addition to the photo-activity, high surface area is also needed [44,45]. The layered porous morphology is also interesting in the supercapacitor application where the high surface area is needed [46]. The electrochemical impedance measurement on the metal oxide nanorods or nanoflakes based electrodes by implementing the scalable solution method indicates enhanced supercapacitance for these morphologies [47,48]. It should also considered that recent studies on CIS and related materials as an electrode for supercapacitor and photo-supercapacitor reveals improved rate capability, remarkable electrochemical stability even at a high current density and high specific capacitance [49]. At the potential of -600 mV, the dense crystalline layer of CIAS can be obtained. The XRD data also validate the higher crystallinity and phase purity of deposited layer at -600 mV (Fig. 6). For comparison, the micrographs, the chemical composition and the XRD diffraction pattern of the layer deposited at room temperature are also provided in Fig. 5 and 6 as well as Table 2.

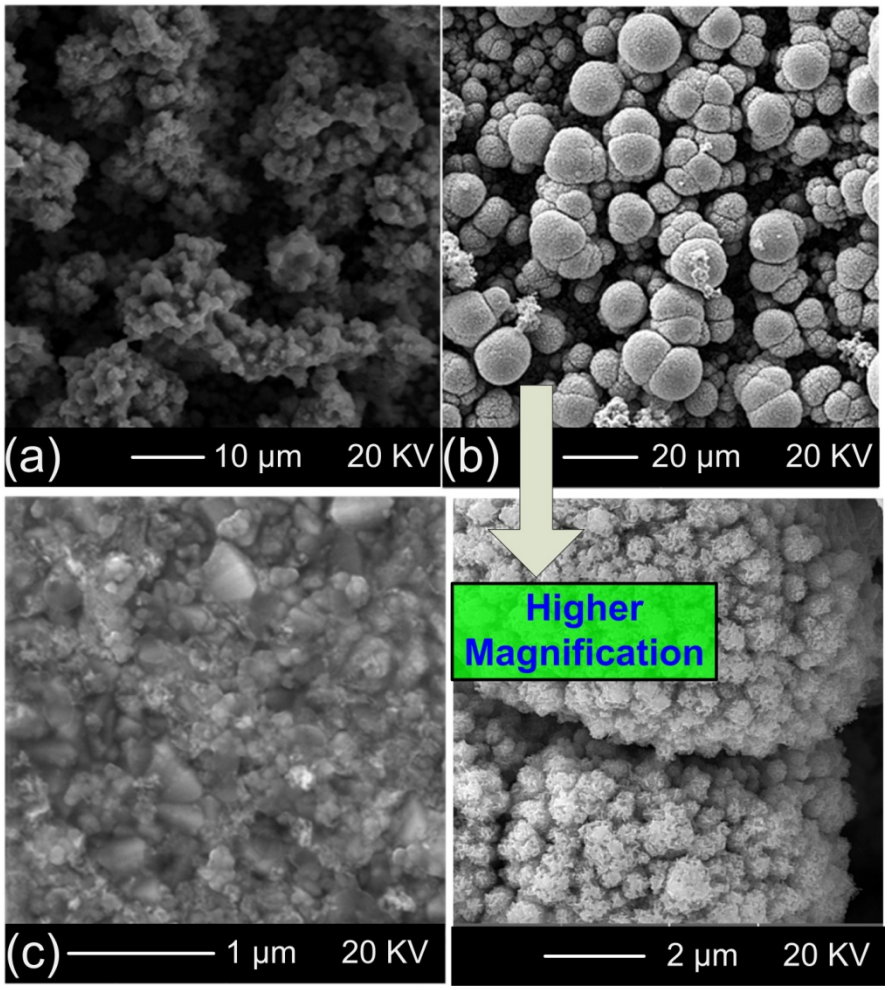

Fig. 5 SEM image of electrodeposited layers prepared at different conditions listed in Table 1; a) RT-700 b) HT-700 and c) HT-600 (comparison of hydrothermal and ambient atmosphere)

Table 2 Composition of the electrodeposited films at room temperature as well as films prepared in hydrothermal condition (120 ^{o}C) with different deposition potentials (the detailed description of all samples is listed in Table 1)

Sample	Cu	Se	In	Al	Composition

RT-700	38.68	57.31	3.15	0.86	$Cu_{1.35}In_{0.11}Al_{0.03}Se_2$
HT-700	36.67	56.72	4.96	1.65	$Cu_{1.29}In_{0.17}Al_{0.05}Se_2$
HT-600	24.22	51.12	18.44	6.22	$Cu_{0.95}In_{0.72}Al_{0.24}Se_2$

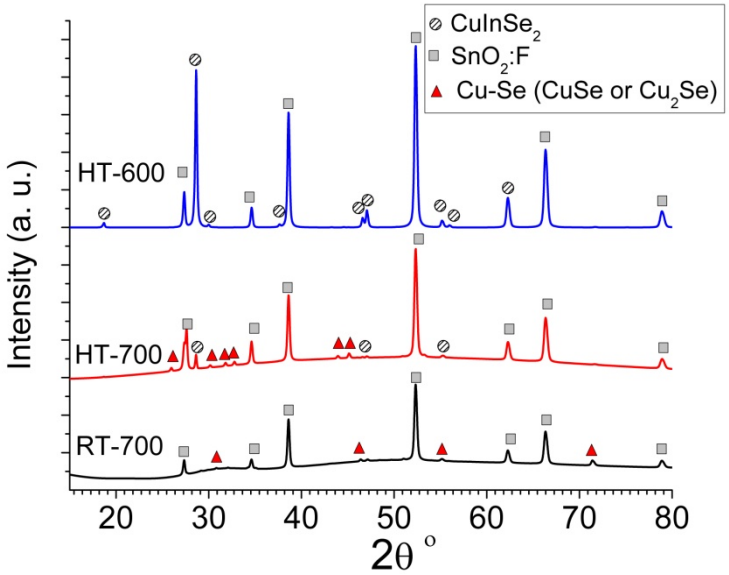

Fig. 6 X-ray diffraction patterns of electrodeposited layers prepared at different conditions listed in Table 1; a) RT-700 b) HT-700 and c) HT-600 (comparison of hydrothermal and ambient atmosphere)

Among all the prepared films, two different samples (RT-700 and HT-600) were selected for post treatment annealing and for following photoresponse measurements. These samples underwent post annealing at 200 ^{o}C in ambient atmosphere, to increase the crystallinity of the as-deposited layers. The post-annealing temperature was selected on the basis of the literature data [50], indeed, a too high temperature would result in the deterioration of the CdS/CIAS heterojunction [4,50]. The microstructures of post-annealed samples have been illustrated in Fig. 7. It can be seen that a dense layer with micronsized grain was obtained after the post treatment annealing of HT-600, while the post-treatment of the former sample (RT-700) produced a rough surface with high porosity which is not suitable for solar cell applications. The compositions of the post-annealed samples are tabulated in Table 3. As expected, the post annealing of HT-600 sample resulted in better stoichiometry due to loss of selenium and the parallel increasing of the percentage of other elements.

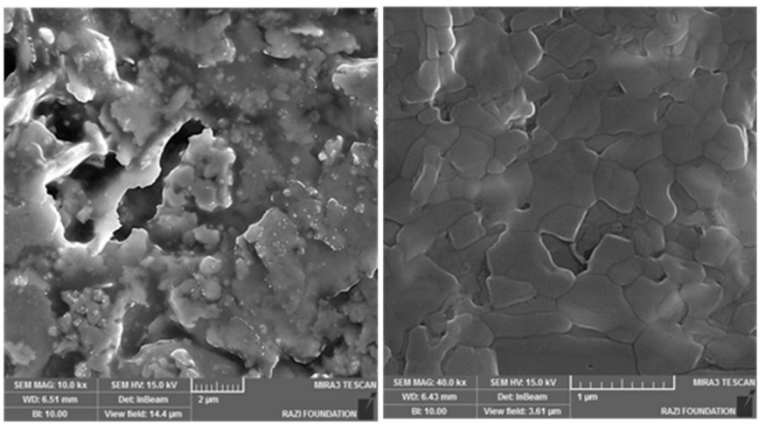

Fig. 7 SEM images of a) **RT-700** b) **HT-600** samples, after post-annealing at 200 ^{o}C (ambient atmosphere)

Table 3 composition of the samples after the post-treatment at 200 °C in ambient atmosphere

Sample	Cu	Se	In	Al	Composition
RT-700	19.39	37.93	36.05	6.63	$Cu_1In_{1.9}Al_{0.35}Se_2$
HT-600	26.03	48.42	24.28	1.27	$Cu_{1.1}In_1Al_{0.05}Se_2$

The photoresponses of the selected samples have been evaluated before and after annealing. The results indicate that all the samples have p-type conductivity. In case of all samples, changes of current with applying negative potential under chopped illumination are observed while the current change after applying positive potential is negligible (See S. Fig. 3 as an example). Then, the photoresponse of the samples was evaluated after applying the potential of -1.0 V under chopped light illumination (Fig. 8 and Table 4). It should be considered that upon light illumination the current density enhanced due to photogenerated electron-hole as charge carrier [25]. As observed, for both samples the photoresponse was enhanced with post annealing at 200 °C. However, post annealed HT-600 sample shows the maximum photoresponse, which is 300 times greater than that of RT-700 sample. High crystallinity, phase purity, enhanced composition and compactness of HT-600 sample result in its superior photoconductivity. The dark current density which is directly proportional with conductivity and carrier concentration are also provided in the Table 4. Results indicate that with post heat treatment the carrier concentration is reduced especially in case of the HT-600 sample. It should be considered that usually electrodeposited CIS layer (and subsequently related materials) have higher carrier concentration in the order of 10^{19} cm^{-3} while carrier densities of well crystalline films with optimized composition is in the range of $1\text{-}2\times10^{16}$ cm^{-3} [25]. For instance it was reported that after treatment in KCN solution the carrier concentration reduced due to improment in the composition [25].

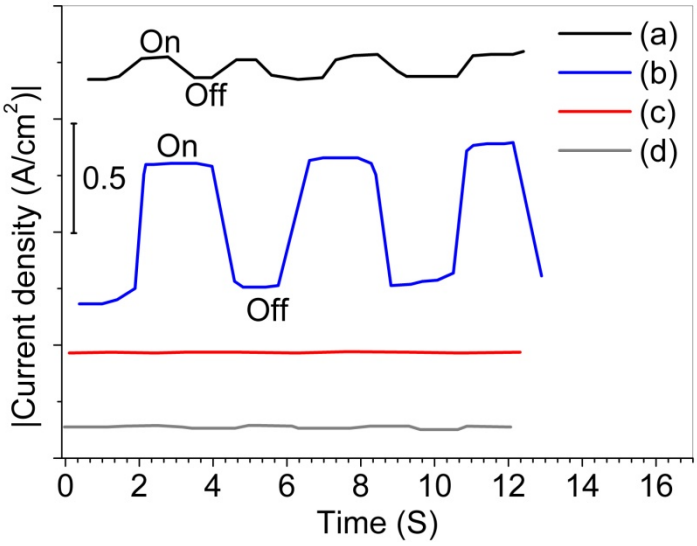

Figure 8 Photoresponse of selected samples recorded under chopped illumination at constant potential of -1.0 V in solution of 1 M NaCl: a) HT-600 sample before post annealing b) HT-600 sample after post-annealing c) RT-700 sample before post annealing d) RT-700 sample after post-annealing (the curves shifted in Y axis for better illustration)

Table 4 Summary of the photo-response investigation of the electrodeposited layers

Sample	Post-annealing condition	Dark current density	Photo-response current	conductivity
HT-600	---	107 μA/cm^2	10 μA/cm^2	P
HT-600	200 ^{o}C (Atm)	10.6 μA/cm^2	60 μA/cm^2	P
RT-700	---	203 μA/cm^2	0.01 μA/cm^2	P
RT-700	200 ^{o}C (Atm)	29.1 μA/cm^2	0.2 μA/cm^2	P

4. Conclusion

In sum, electrodeposition of CIAS from quaternary Cu, In, Al and Se aqueous solutions has been performed at different temperatures. It was found that properties of electrodeposited layer are greatly improved at high temperature. For this reason, a combination of hydrothermal and electrodeposition methods has been employed for preparation of CIAS thin films and it was observed that highly crystalline CIAS thin films with micron-sized grains and superior photoconductivity (60 μA/cm^2) can be obtained by a simple post-treatment annealing of these samples.

5. Acknowledgment

Authors would like to thanks Prof. Silvia Bordiga from University of Turin for support of the research.

References

1. Kennedy J, Murmu P, Gupta P, Carder D, Chong S, Leveneur J, Rubanov S (2014) Effects of annealing on the structural and optical properties of zinc sulfide thin films deposited by ion beam sputtering. Materials Science in Semiconductor Processing 26:561-566.
2. Kaviyarasu K, Ayeshamariam A, Manikandan E, Kennedy J, Ladchumananandasivam R, Gomes UU, Jayachandran M, Maaza M (2016) Solution processing of CuSe quantum dots: Photocatalytic activity under RhB for UV and visible-light solar irradiation. Materials Science and Engineering: B 210:1-9.
3. Frontier S (2015) Solar Frontier achieves world record thin-film solar cell efficiency: 22.3%. Press Release.
4. Shafarman WN, Stolt L (2003) Cu(InGa)Se_2 Solar Cells. In: Luque A, Hegedus S (eds) Handbook of Photovoltaic Science and Engineering. John Wiley & Sons, England, pp 568-618
5. Huang Q, Reuter K, Amhed S, Deligianni L, Romankiw L, Jaime S, Grand P-P, Charrier V (2011) Electrodeposition of indium on copper for CIS and CIGS solar cell applications. Journal of The Electrochemical Society 158:D57-D61.
6. Saji VS, Choi I-H, Lee C-W (2011) Progress in electrodeposited absorber layer for $CuIn_{(1-x)}Ga_xSe_2$ (CIGS) solar cells. Solar Energy 85:2666-2678.
7. Woods LM, Kalla A, Gonzalez D, Ribelin R (2005) Wide-bandgap CIAS thin-film photovoltaics with transparent back contacts for next generation single and multi-junction devices. Materials Science and Engineering: B 116:297-302.
8. Sheppard C, Alberts V (2006) Deposition of single-phase CuIn(Se, $S)_2$ thin films from the sulfurization of selenized CuIn alloys. Journal of Physics D: Applied Physics 39 (17):3760.
9. Birkmire RW (2001) compound polycrystalline solar cells: Recent progress and Y2K perspective. Solar Energy Materials and Solar Cells 65:17-28.
10. Marsillac S, Paulson PD, Haimbodi MW, Birkmire RW, Shafarman WN (2002) High-efficiency solar cells based on $CuInAlSe_2$ thin films. Applied Physics Letters 81:1350-1352.
11. Nahory R, Pollack M, Johnston Jr W, Barns R (1978) Band gap versus composition and demonstration of Vegard's law for $In_{1-x}Ga_xAs_yP_{1-y}$ lattice matched to InP. Applied Physics Letters 33:659-661.
12. Markwitz A, Kennedy J (2009) Group-IV and V ion implantation into nanomaterials and elemental analysis on the nanometre scale. International Journal of Nanotechnology 6:369-383.

13. Christie V, Liem S, Reeves R, Kennedy V, Markwitz A, Durbin S (2004) Characterisation of polycrystalline gallium nitride grown by plasma-assisted evaporation. Current Applied Physics 4:225-228.
14. Deepa KG, Shruthi NL, Sunil MA, Nagaraju J (2014) Cu(In,Al)Se_2 thin films by one-step electrodeposition for photovoltaics. Thin Solid Films 551:1-7.
15. Prasher D, Rajaram P (2011) Growth and characterization of electrodeposited Cu(In,Al)Se_2 thin films. Thin Solid Films 519:6252-6257.
16. Huang K-C, Liu C-L, Hung P-K, Houng M-P (2013) Effect of [Al] and [In] molar ratio in solutions on the growth and microstructure of electrodeposition Cu(In,Al)Se_2 films. Applied Surface Science 273:723-729.
17. Huang K-C, Liu C-L, Hung P-K, Houngz M-P (2013) Cyclic Voltammetric Study and Nucleation of Electrodeposited Cu(In,Al)Se_2 Thin Films with Sodium Dodecyl Sulfate Additive. Journal of The Electrochemical Society 160:D125-D131.
18. Prasher D, Sharma R, Sharma AK, Rajaram P (2011) $CuIn_{1-X}Al_XSe_2$ Thin Films Grown By Electrodeposition. AIP Conference Proceedings 1349:597-598.
19. Huang K-C, Liu C-L, Hung P-K, Houng M-P (2014) Influence of copper concentration in solutions on the growth mechanism and performance of electrodeposited Cu(In,Al)Se_2 solar cells. Solar Energy Materials & Solar Cells 128:27-35.
20. Lincot D (2005) Electrodeposition of semiconductors. Thin Solid Films 487:40- 48.
21. Bp Global, statistical review of world energy June 2014, (www.bp.com, last accessed August 2014).
22. Bouabid K, Ihlal A, Manar A, Outzourhit A, Ameziane EL (2005) Effect of deposition and annealing parameters on the properties of electrodeposited $CuIn_{1-x}Ga_x$ thin films. Thin Solid Films 488:62-67.
23. Garg P, Garg A, Rastogi AC, Garg JC (1991) Growth and characterization of electrodeposited $CuInSe_2$ thin films from seleno-sulphate solution. Journal of Physics D: Applied Physics 24:2026-2031.
24. Thouin L, Massaccesi S, Sanchez S, Vedel J (1994) Formation of copper indium diselenide by electrodeposition. Journal of Electroanalytical Chemistry 374:81-88.
25. Kemell M (2003) Electrodeposition of $CuInSe_2$ and doped ZnO thin films for solar cells. University of Helsinki, Helsinki
26. Kemell M, Ritala M, Leskela M (2001) Effects of post-deposition treatments on the photoactivity of $CuInSe_2$ thin fims deposited by the induced co-deposition mechanism. Journal of Materials Chemistry 11:668-672.
27. Kessler F, Herrmann D, Powalla M (2005) Approaches to flexible CIGS thin-film solar cells. Thin Solid Films 480-481:491-498.
28. Ganjkhanlou Y, Ebadzadeh T, Kazemzad M, Maghsoudipour A, Kianpour-Rad M (2015) Effect of pH on the electrodeposition of Cu(In, Al)Se_2 from aqueous solution in presence of citric acid as complexing agent. Surface Review and Letters 22:1550057.
29. Contreras MA, Romero MJ, To B, Hasoon F, Noufi R, Ward S, Ramanathan K (2002) Optimization of CBD CdS process in high-efficiency Cu(In,Ga)Se_2-based solar cells. Thin Solid Films 403-404:204-211.
30. Nakada T, Okano N, Tanaka Y, Fukuda H, Kunioka A Superstrate-type $CuInSe_2$ solar cells with chemically deposited CdS window layers. In: Photovoltaic Energy Conversion, 1994., Conference Record of the Twenty Fourth. IEEE Photovoltaic Specialists Conference-1994, 1994. IEEE, pp 95-98
31. Cao Q, Gunawan O, Copel M, Reuter KB, Chey SJ, Deline VR, Mitzi DB (2011) Defects in Cu (In, Ga)Se_2 chalcopyrite semiconductors: a comparative study of material properties, defect states, and photovoltaic performance. Advanced Energy Materials 1:845-853.
32. Izquierdo-Roca V, Fontane X, Saucedo E, Jaime-Ferrer JS, Alvarez-Garcıa J, Perez-Rodrıguez A, Bermudez V, Morante JR (2011) Process monitoring of chalcopyrite photovoltaic technologies by Raman spectroscopy: an application to low cost electrodeposition based processes. New Journal of Chemistry 35:453-460.
33. Olejna□ek J, Kamler CA, Darveau SA, Exstrom CL, Slaymaker LE, Vandeventer AR, Ianno NJ, Soukup RJ (2011) Formation of $CuIn_{1-x}Al_xSe_2$ thin films studied by Raman scattering. Thin Solid Films 519:5329-5334.
34. Kennedy J, Sundrakannan B, Katiyar R, Markwitz A, Li Z, Gao W (2008) Raman scattering investigation of hydrogen and nitrogen ion implanted ZnO thin films. Current Applied Physics 8:291-294.
35. Kennedy J, Murmu P, Leveneur J, Markwitz A, Futter J (2016) Controlling preferred orientation and electrical conductivity of zinc oxide thin films by post growth annealing treatment. Applied Surface Science 367:52-58.

36. Kennedy J, Murmu P, Manikandan E, Lee S (2014) Investigation of structural and photoluminescence properties of gas and metal ions doped zinc oxide single crystals. Journal of Alloys and Compounds 616:614-617.
37. Lee H, Lee J-H, Hwang Y-H, Kim Y (2014) Cyclic voltammetry study of electrodeposition of $CuGaSe_2$ thin films on ITO-glass substrates. Current Applied Physics 14:18-22.
38. Liu F, Huang C, Lai Y, Zhang Z, Li J, Liu Y (2011) Preparation of $Cu(In,Ga)Se_2$ thin films by pulse electrodeposition. Journal of Alloys and Compounds 509:L129-L133.
39. Balantseva E, Camino B, Ferrari AM, Berlier G (2015) Effect of post-synthesis treatments on the properties of ZnS nanoparticles: an experimental and computational study. Oil & Gas Science and Technology–Revue d'IFP Energies nouvelles 70:817-829.
40. Lee J-W, Son D-Y, Ahn TK, Shin H-W, Kim IY, Hwang S-J, Ko MJ, Sul S, Han H, Park N-G (2013) Quantum-Dot-Sensitized Solar Cell with Unprecedentedly High Photocurrent. Scientific Reports 3:1050.
41. Bulánek R, Čapek L, Setnička M, Čičmanec P (2011) DR UV–Vis study of the supported vanadium oxide catalysts. The Journal of Physical Chemistry C 115:12430-12438.
42. Kavitha B, Dhanam M (2007) In and Al composition in nano-$Cu(InAl)Se_2$ thin films from XRD and transmittance spectra. Materials Science and Engineering: B 140:59-63.
43. Yamada S, Tanaka K, Minemoto T, Takakura H (2009) Effect of Al addition on the characteristics of $Cu(In,Al)Se_2$ solar cells. Journal of Crystal Growth 311:731-734.
44. Kaviyarasu K, Manikandan E, Kennedy J, Jayachandran M, Ladchumananandasiivam R, De Gomes UU, Maaza M (2016) Synthesis and characterization studies of NiO nanorods for enhancing solar cell efficiency using photon upconversion materials. Ceramics International 42:8385-8394.
45. Mali MG, Yoon H, Joshi BN, Park H, Al-Deyab SS, Lim DC, Ahn S, Nervi C, Yoon SS (2015) Enhanced photoelectrochemical solar water splitting using a platinum-decorated CIGS/CdS/ZnO photocathode. ACS applied materials & interfaces 7:21619-21625.
46. Dabaghi HH, Kazemzad M, Ganjkhanlou Y, Eskandari R (2013) Preparation Of Nickel Oxide Embedded Self Organized Titania Nanotubes Array By New Alginate Method As A Supercapacitor Electrode. Surface Review and Letters 20:1350062.
47. Kaviyarasu K, Premanand D, Kennedy J, Manikandan E (2013) Synthesis of Mg doped TiO_2 nanocrystals prepared by wet-chemical method: optical and microscopic studies. International Journal of Nanoscience 12:1350033.
48. Rakhi R, Chen W, Hedhili MN, Cha D, Alshareef HN (2014) Enhanced rate performance of mesoporous Co_3O_4 nanosheet supercapacitor electrodes by hydrous RuO_2 nanoparticle decoration. ACS applied materials & interfaces 6:4196-4206.
49. Ng C, Lim H, Hayase S, Harrison I, Pandikumar A, Huang N (2015) Potential active materials for photo-supercapacitor: A review. Journal of Power Sources 296:169-185.
50. Mickelsen R, Chen W Development of a 9.4% efficient thin-film $CuInSe_2$/CdS solar cell. In: 15th Photovoltaic Specialists Conference, 1981. pp 800-804